nature communications

Article

https://doi.org/10.1038/s41467-024-50778-z

The constant oxidation state of Earth's mantle since the Hadean

Received: 7 February 2024

Accepted: 19 July 2024

Published online: 10 August 2024

Check for updates

Fangyi Zhang [1] ✉, Vincenzo Stagno [2], Lipeng Zhang [1,3], Chen Chen[1], Haiyang Liu [1], Congying Li[1,3] & Weidong Sun [1,3,4] ✉

Determining the evolutionary history of mantle oxygen fugacity (fO_2) is crucial, as it controls the fO_2 of mantle-derived melts and regulates atmospheric composition through volcanic outgassing. However, the evolution of mantle fO_2 remains controversial. Here, we present a comprehensive dataset of plume-derived komatiites, picrites, and ambient mantle-derived (meta)basalts, spanning from ~3.8 Ga to the present, to investigate mantle thermal and redox states evolution. Our results indicate that fO_2 of both mantle plume-derived and ambient mantle-derived melts was lower during the Archean compared to the post-Archean period. This increase in the fO_2 of mantle-derived melts over time correlates with decreases in mantle potential temperature and melting depth. By normalizing fO_2 to a constant reference pressure (potential oxygen fugacity), we show that the fO_2 of both the mantle plume and ambient upper mantle has remained constant since the Hadean. These findings suggest that secular mantle cooling reduced melting depth, increasing the fO_2 of mantle-derived melts and contributing to atmospheric oxygenation.

The mantle constitutes the most significant volatile reservoir on Earth, and the release of volatiles (e.g. H, C, O, and S) through volcanic degassing governs the composition of the atmosphere[1,2]. During the migration of volatiles from the mantle to the atmosphere, temperature, and oxygen fugacity (fO_2) have emerged as critical parameters controlling the speciation and concentration of volatiles in volcanic gases[3,4]. Temperature plays a pivotal role in determining the depth and extent of partial melting within the mantle, thereby influencing the chemical composition and volatile content of magma[5,6]. Concurrently, fO_2 directly affects the composition of volcanic gases by governing the valence states of volatile elements[7]. Therefore, to elucidate the composition of the atmosphere, conducting a comprehensive examination of the thermal and redox state evolution of the mantle over time is critical[1,8].

Petrological and theoretical investigations of the thermal state of the mantle have established a consensus that the mantle has been cooling since the Archean[9–12]. The prevalence of komatiites and high-MgO basalts during the Archean era points to substantially higher potential temperatures (T_P) and greater melting degrees in the mantle compared to present-day conditions. However, the evolutionary history of the mantle redox state remains controversial, given the scarcity of both preserved effusive rocks and accurately dated mantle peridotites and eclogites[13,14]. The consistent V/Sc ratios observed in the Archean and modern basalts suggest that the mantle fO_2 has been constant since the early Archean[15]. This perspective is reinforced by the cerium anomalies in Hadean zircons, which indicate that mantle fO_2 reached modern levels around 4.3 billion years ago[16]. However, this finding is subject to significant uncertainty, which may obscure potential oxidative trends. In contrast, recent studies on Archean eclogites as proxies for basalts[17], Archean basalts[18], and ultramafic lavas (komatiites and picrites[19]) suggest an increase in mantle fO_2 of over one log unit from approximately 3.8 Ga. Nonetheless, these studies infer mantle redox evolution based on the fO_2 of mantle-derived magmas, which depends not only on fO_2 buffered by mantle minerals but also on the depth and degree of melting[20,21]. The petrological and experimental results suggest that the mantle redox state is expected to

[1]Center of Deep Sea Research, Institute of Oceanology, Chinese Academy of Sciences, Qingdao 266071, China. [2]Department of Earth Sciences, Sapienza University of Rome, Rome, Italy. [3]Laoshan Laboratory, Qingdao 266237, China. [4]University of the Chinese Academy of Sciences, Beijing 100049, China. ✉e-mail: zhangfy@qdio.ac.cn; weidongsun@qdio.ac.cn

decrease with depth[7,22,23]. Therefore, variations in the redox state of mantle-derived melts may not necessarily reflect changes in mantle fO_2, but rather the depth at which the melts were extracted from the mantle source. Given that the melt extraction depth is significantly influenced by the mantle potential temperature[24], it is imperative to correct for the temperature and pressure effects on the fO_2 of mantle-derived melts when exploring the intrinsic redox state of the mantle.

In this study, we present a comprehensive compilation of two distinct databases. The first database encompasses global whole-rock compositions of primitive non-arc basalts, as well as mantle and orogenic eclogite suites, covering a period from 3.8 to 0 Ga[17,18,25]. Utilizing geochemical criteria, such as less fractionated mafic samples, high Nb/La ratios, low loss on ignition and high CaO content, we selectively analyzed primitive basalts from peridotite sources to gain insights into the evolution of fO_2 within the shallow ambient mantle (refer to Methods for details). The second database includes a global collection of whole-rock and olivine compositions from ultramafic lavas (komatiites and picrites) ranging from 3.6 to 0 Ga. These rocks, identified as being derived from high-temperature mantle plumes[11,26], facilitate the investigation of fO_2 evolution of deep mantle plumes. By applying a combination of thermobarometers[24,27,28] and oxybarometers[29–31] to samples from diverse reservoirs, we systematically investigated the temporal variations in the mantle's thermal state, melting depth, and redox state.

Results and discussion

Evolution of thermal and redox states of mantle-derived magmas

There is consensus that the mantle has undergone gradual cooling since the Archaean[10–12]. In this study, we investigated the melting temperatures and pressures inferred from mid-ocean ridge basalt (MORB)-like basalts. Our results reveal that the T_P of the ambient mantle rose from approximately 3.8 Ga, reaching peak values of around 1510 ± 80 °C (1σ) during 2.7–3.3 Ga, before a steady decline to the current value of 1350 °C (Fig. 1a). This concave thermal evolution curve is consistent with the low-Urey-ratio model (present-day Urey ratio 0.23–0.34), implying an initial heating phase followed by cooling, with peak T_P occurring around 2.7–3.3 Ga[9,11].

The reconstructed primary Archean komatiites exhibited high MgO content, ranging from 25 to 31 wt.%, while the primary Phanerozoic plume-derived magmas contained 12–25 wt.% MgO. This indicates a significantly elevated mantle potential temperature during the Archean period[32]. Thermobarometric results revealed that Archean komatiites recorded T_P between 1700 and 1800 °C (Fig. 1a), exceeding the potential temperature of the Archean ambient mantle by over 100 °C, thereby corroborating their plume origin[11]. Moreover, the potential temperature of mantle plumes shows a slight increase from around 3.6 to 3.3 Ga, followed by a gradual decrease from approximately 2.7 Ga to the present (Fig. 1a). Both ambient mantle and mantle plumes exhibit concave thermal evolution curves peaking at 2.7–3.3 Ga, which aligns with current Urey ratios of 0.08 to 0.34, respectively[9,11]. The consistent cooling paths for both the ambient mantle and mantle plumes suggest parallel cooling histories for the shallow and deep mantles. From the Hadean to the Archean, the internal heating of the mantle surpassed surface heat loss, resulting in mantle warming. After the Archean, increased surface heat loss led to gradual mantle cooling[33]. Additionally, our pressure-temperature estimates indicate a direct correlation between the melting pressures of mantle-derived magmas and the mantle potential temperature, with peak melting pressures occurring around 2.7–3.3 Ga. These findings indicate a secular cooling trend of the mantle and a decrease in the melt extraction depth from the Archean to the present.

We employed diverse methods to calculate fO_2 for different rock types. For plume-derived magmas, we utilized $D^{Ol/melt}_V$ oxybarometers,

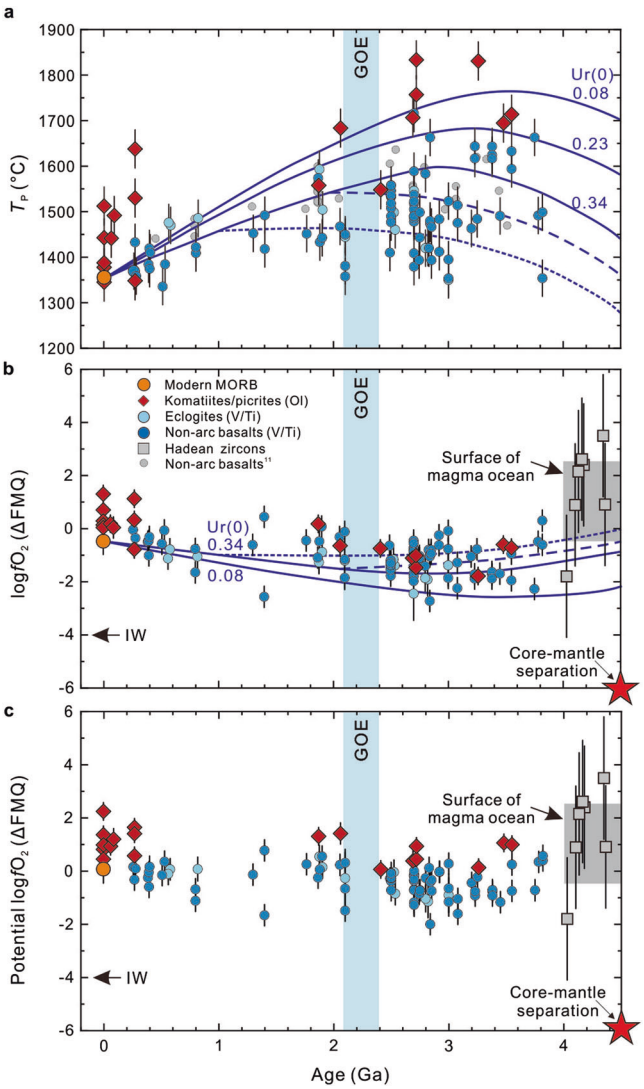

Fig. 1 | Secular thermal and redox states evolution of mantle-derived melts. **a** The mantle potential temperatures (T_P) of mantle plume and ambient mantle estimated from thermometer[24]. Blue solid lines represent the thermal evolution of the mantle with different present-day Urey ratio (Ur(0), and blue dashed and dotted lines represent the switch from stagnant lid convection to plate tectonics at 2 Ga and 1 Ga[33], respectively. **b** Calculated fO_2 of mantle plume- and ambient mantle-derived melts relative to the fayalite–magnetite–quartz (ΔFMQ) buffer. The fO_2 of mantle plume-derived melts was determined using the partition of V between olivine and melts[29] ($D^{ol/melt}_V$), the fO_2 of ambient mantle-derived melts was estimated by V-Ti redox proxy[18]. The fO_2 of modern MORB is shown[63,64]. Blue solid lines represent the fO_2 evolution trend estimated from the thermal evolution model with different Ur(0) (see Methods). **c** The fO_{2P} of a mantle plume and ambient mantle remain constant since the Hadean. The timing of the Great Oxidation Event (GOE) and the fO_2 of Hadean mantle-derived zircons[16] are shown for comparison. The fO_2 of the mantle in equilibrating with the core was estimated to ΔFMQ −6[7]. All the results are presented as mean values ± standard deviation (1σ).

whereas for ambient mantle-derived magmas lacking preserved olivine, we used a whole-rock V/Ti redox proxy. These methods are highly regarded for their precision in determining fO_2[19,29,30]. The results of the $D^{Ol/melt}_V$ oxybarometer reveal that the fO_2 of mantle plume-derived melts from the Archean was significantly lower, at ΔFMQ −1.11 ± 0.45 (1σ; ΔFMQ indicating the fO_2 after subtracting the fO_2 for the fayalite–magnetite–quartz buffer), compared to post-Archean samples, which exhibited fO_2 values of ΔFMQ + 0.17 ± 0.64 (Fig. 1b). This trend is consistent with previous studies on the fO_2 of mantle plumes-derived melts[19]. To statistically analyze the differences in fO_2 between

https://doi.org/10.1038/s41467-024-50778-z

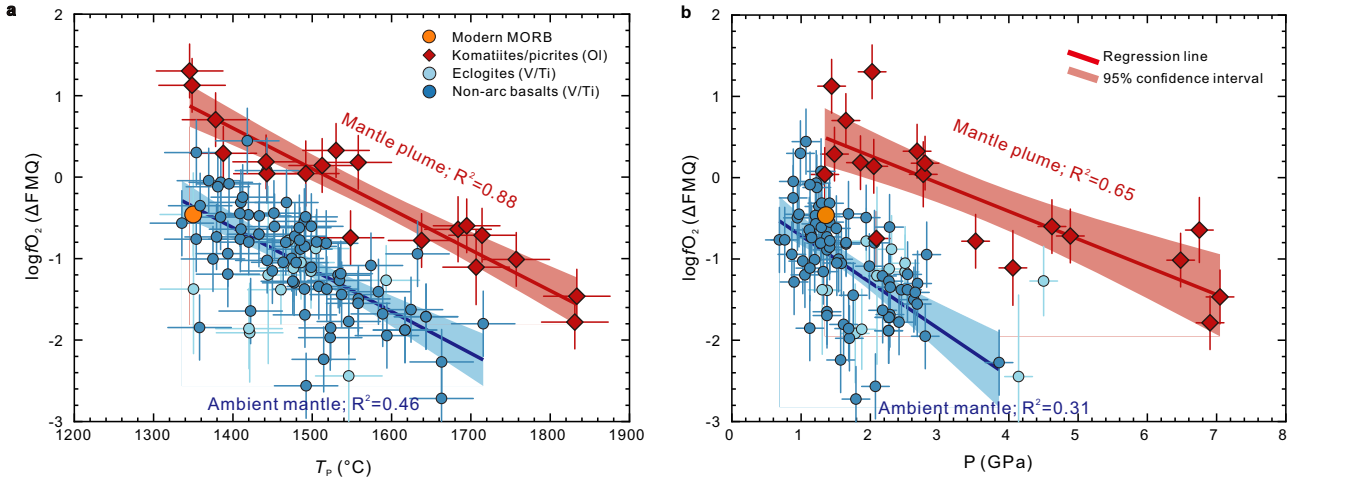

Fig. 2 | Correlations between the fo_2 of mantle derived melts and melting conditions. a The fo_2 plot against T_P. **b** The fo_2 plot against melting pressure. T_P and melting pressure are calculated by the thermobarometers[24,27]. The solid lines and error bands represent regression lines and 95% confidence intervals, respectively. Both plume and ambient-derived melts exhibit a strong inverse correlation between T_P, melting pressure, and fo_2, suggesting that the fo_2 of mantle-derived melts is controlled by the thermal state of the mantle. The error bars for all results are 1σ.

the Archean and post-Archean samples, we conducted a Student's *t*-test. The average *P*-value of the two-sample t-tests was less than 0.01, indicating that the null hypothesis of consistent fo_2 values between the Archean and post-Archean mantle plume-derived melts can be rejected. A similar evolutionary trend was observed in ambient mantle-derived magmas, with Archean samples showing significantly lower fo_2 at ΔFMQ −1.21 ± 0.59 compared to ΔFMQ −0.66 ± 0.67 in post-Archean samples ($P < 0.01$). Our findings demonstrate that the fo_2 of both the mantle plume and ambient mantle-derived magmas increased by approximately 1 log unit from the Archean to the Phanerozoic[17,19]. Notably, since the Archean, the increase in magma fo_2 has been accompanied by a reduction in the mantle potential temperature, suggesting a potential correlation between magma fo_2 and the thermal state of the mantle.

The constant oxidation state of the mantle over time

Numerous studies have demonstrated that the fo_2 of the upper mantle decreases with depth, which is attributed to the increased stability of Fe^{3+} in garnet and then in majorite at high pressure[7,20,34]. During adiabatically upwelling, the mantle fo_2 will increase with decreasing depth even if the bulk rock $Fe^{3+}/\Sigma Fe$ ratio is constant[20]. Therefore, the fo_2 of the mantle-derived magma is not only controlled by the intrinsic redox state of the mantle source rock ($Fe^{3+}/\Sigma Fe$ ratio of the mantle), but also by the melt extraction depth[21]. By comparing the secular evolution of the redox and thermal states of mantle-derived magmas, we found that the fo_2 of these magmas was negatively correlated with both T_P and melting pressure (Fig. 2). This negative correlation suggests that the fo_2 of mantle-derived magma may be significantly influenced by the depth of melt extraction.

Komatiites are ultramafic rocks that formed under exceptionally high temperature (>1600 °C) and pressure conditions (>4 GPa), predominantly during the Archean era when T_P was elevated[26,35]. These magmas, originating from deep within the mantle, are characterized by low fo_2[36,37]. As shown in Fig. 3, the mantle sources of komatiites display low fo_2 when corrected to the pressure and temperature of melt extraction, ranging from FMQ −2 to 0. However, considering the link between mantle fo_2 and depth, the bulk mantle $Fe^{3+}/\Sigma Fe$ ratios for komatiite sources were deduced to be 5–10% (Fig. 3b). These ratios align with those proposed for mantle plumes during the Phanerozoic[38,39], indicating the intrinsic redox state of mantle plumes has remained relatively unchanged since the Archean.

To mitigate the effect of melting depth on magma fo_2 and elucidate the intrinsic redox evolution of the mantle, we introduced the concept of potential oxygen fugacity (fo_{2P}). This concept is analogous to the canonical definition of T_P[40] and represents the fo_2 that the mantle would exhibit if it were to rise adiabatically to the depth of MORB extraction (1 GPa) along a solid adiabat without undergoing melting (Fig. 3b). The knowledge of fo_{2P} requires calculating the fo_2 of the mantle source and estimating the variation of fo_2 from the melting depth to 1 GPa along an adiabat[20] (Methods).

Through the correction of the fo_2 of various mantle-derived melts to fo_{2P}, we observe that both the fo_{2P} of the ambient mantle and mantle plumes have the same fo_2 (−1 < ΔFMQ < +1), and this value has remained constant since the early Archean (Fig. 1c). These findings are identical to the fo_2 record in Hadean zircons[16]. In addition, experimental studies and first principles simulations shed light on the behavior of Fe^{2+} in the Earth's deep magma ocean, demonstrating its disproportionation to Fe^{3+} and Fe metal. The non-equilibrium percolation of disproportionation-derived metallic iron into the core, led to upper mantle oxidation, removing the core and mantle from redox equilibrium, as observed in the present day[41–44]. For large-volume planets, such as the Earth, with deep magma oceans, fo_2 at the surface of the magma ocean likely reached present-day mantle levels (Fig. 1c). These insights, combined with petrological evidence[45], confirm that the mantle achieved modern oxidation levels and has maintained a redox gradient since the Hadean period. The thermal state of the mantle evolved continuously, affecting the depth and extent of partial melting and consequently altering the fo_2 of mantle-derived magmas.

Estimating the fo_2 of Hadean crust

The strong correlation between the fo_2 of mantle-derived magma and mantle T_P provides an opportunity to model the fo_2 of the crust in the Hadean eon when the petrologic record is sparse[16]. It has been suggested that radiogenic heat production in the mantle exceeded surface heat loss; thus, the mantle warmed from the Hadean to the Archean[9,11,33]. Based on the possible T_P during the Hadean (Urey ratio of 0.08 to 0.34), we predict oxidized conditions for mantle-derived melts in the Hadean, corresponding to fo_2 values of ΔFMQ −1 to +1 (Fig. 1b).

Hadean zircons constitute the primary geological record of the Hadean. Although these zircons crystallized from differentiated felsic melts rather than directly from mantle-derived magmas, the relative

https://doi.org/10.1038/s41467-024-50778-z

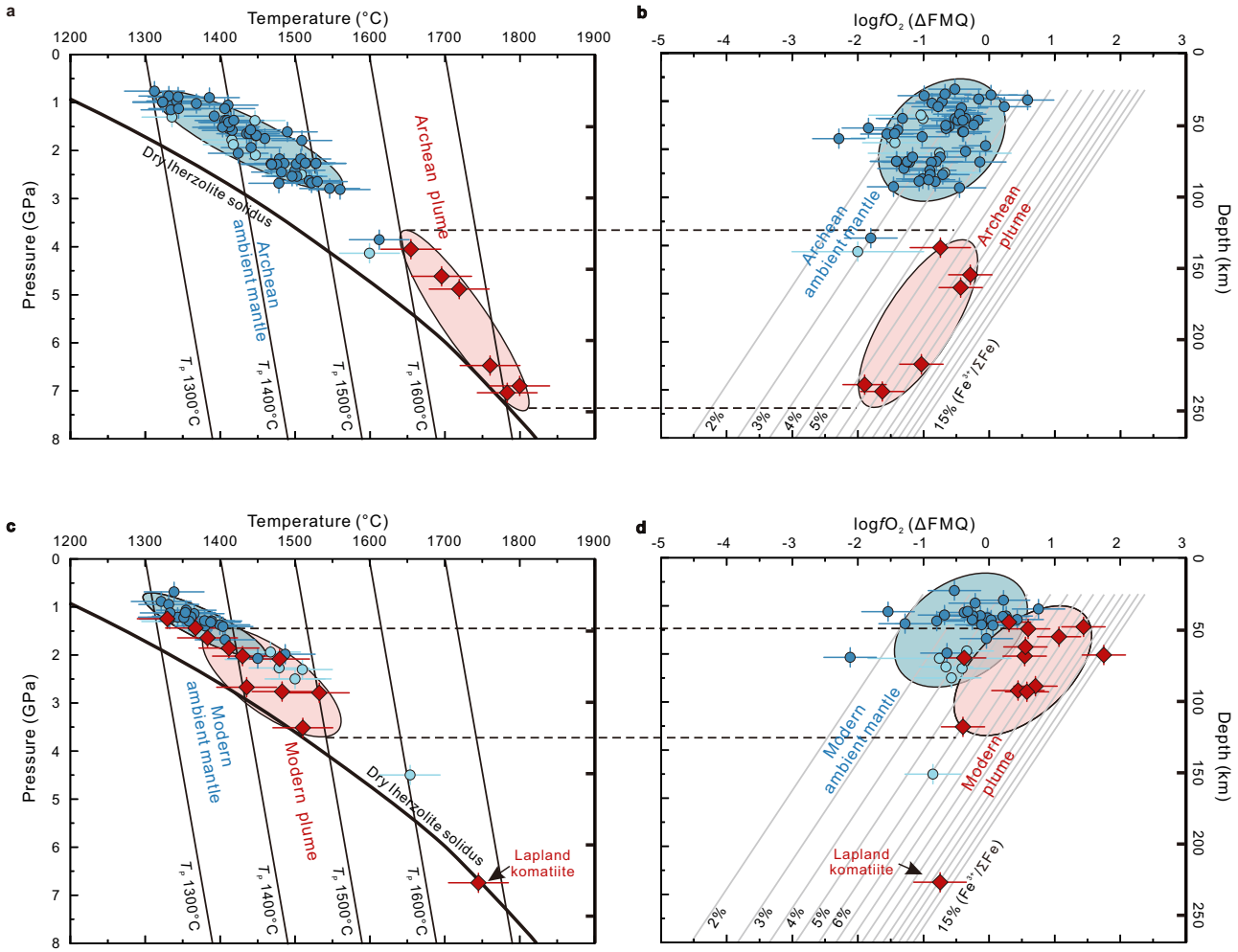

Fig. 3 | Temperature–pressure and oxygen fugacity of the mantle source for mantle-derived melts. Average temperatures and pressures of partial melting for Archean (**a**) and Phanerozoic magmas (**b**). The relationship between melting pressure and fo_2 of the mantle for Archean (**c**) and Phanerozoic magmas (**d**). The parallel grey lines represent the fo_2 of the mantle with different $Fe^{3+}/\Sigma Fe$ ratios calculated by the thermodynamic model[20]. The fo_2 of mantle-derived melts have been corrected to their respective source conditions. The error bars for all results are 1σ and the legends and symbols as in Fig. 1.

changes in fo_2 along the magmatic liquid lines of descent are typically on the order of 1–2 log unit[16]. Therefore, the fo_2 values recorded in these zircons can provide valuable insights into the fo_2 of Hadean mantle-derived magmas. Systematic studies of zircons reveal that those older than 4.0 Ga have recorded an fo_2 of −0.33 ± 0.86[46]. Notably, zircons with mantle oxygen isotope characteristics display relatively high fo_2 values (ΔFMQ + 1.4 ± 2.0)[16]. These observations support our predictions and suggest a colder, more oxidized crust during the Hadean eon. The oxidized Hadean crust likely played a vital role in the formation of oxidized fluids within early terrestrial hydrothermal systems by facilitating prebiotic molecular synthesis and supplying essential nutrients for early life.

Secular cooling of the mantle prompts atmospheric oxygenation

It has been hypothesized that secular oxidization of the mantle since the Archean facilitated the oxygenation of the atmosphere, leading to the Great Oxidation Event at 2.4–2.2 Ga[8,17,19]. However, our study reveals a more nuanced perspective, indicating that the fo_2 of mantle-derived magmas, which facilitates volatile transfer between the mantle and atmosphere, experienced a gradual increase. This increase, however, is not due to mantle oxidation but is largely influenced by changes in the thermal state of the mantle, which affected the average melting depth and extent (Fig. 4). This insight highlights the complex interplay among the mantle thermal state, magma evolution, and the redox evolution of the Earth's atmosphere.

Methods

Data collection and filtration

To obtain the thermal and redox evolution trend of the mantle, we collected olivine and corresponding whole-rock trace element compositions of well-preserved picrites and komatiites. The ultramafic lavas have been demonstrated to be related to hot mantle plumes and to preserve fresh olivines[11,26,32,47], including Reykjanes Peninsula picrites from Iceland (0 Ga), Kilauea picrites from Hawaii (0 Ga), Padloping picrites from Baffin Island (0.062 Ga), Gorgona komatiites from Gorgona Island (0.089 Ga), Dali and Lijiang picrites from Emeishan (0.26 Ga), Winnipegosis komatiites from the Superior Craton (1.87 Ga), Lapland komatiites (2.06 Ga) and Vetreny komatiites (2.41 Ga) from the Fennoscandian Shield, Belingwe komatiites from the Rhodesian Craton (2.69 Ga), Pyke Hill and Alexo komatiites from Abitibi greenstone belt in Canadian Shield (2.72 Ga), Weltevreden komatiites (3.26 Ga), Komati komatiites (3.48 Ga) and Schapenburg komatiite (3.55 Ga) from Barberton Greenstone Belt in Kaapvaal Craton. Details for the sample descriptions and references are provided in Supplementary data 1.

https://doi.org/10.1038/s41467-024-50778-z

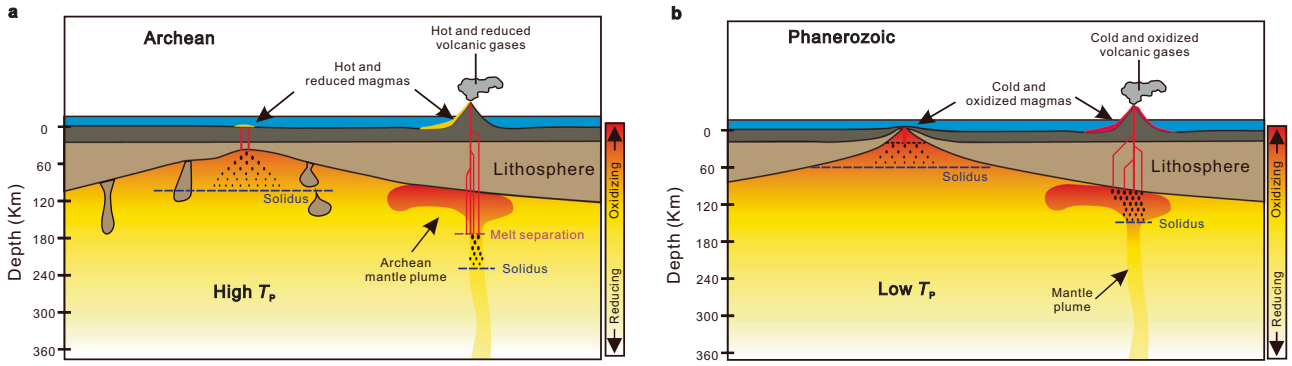

Fig. 4 | Redox state of mantle-derived melts controlled by the thermal state of the mantle. Cartoon illustrating the higher T_P in Archean caused deeper and more extensive melting of the mantle, resulting in lower fo_2 of Archean magmas (**a**). In contrast, the lower T_P during the Phanerozoic led to shallower melts with higher oxidation due to the mantle's redox structure[20,31] (**b**). The concurrent cooling and oxidation of mantle-derived melts at the end of the Archean played a crucial role in transforming volcanic gases from an anoxic to an oxic state, potentially triggering atmospheric oxygenation. The stagnant-lid tectonic regime in Archean was from ref. 65.

Given the scarcity of olivine trace element data for Archean basalts, we compiled a whole-rock composition dataset of 3.8-0 Ga modern MORB-like basalts to investigate the fo_2 of the ambient mantle by V/Ti redox proxy. The whole-rock geochemical data of the basalts were assembled from the EarthChem rock database, the database collected by ref. 25 and the Archean basalt database[18]. To filter MORB-like basalts, we used several criteria as follows: (1) we screened basalts with SiO_2 contents ranging from 45 to 54 wt.%. (2) Samples with MgO content of <8 wt.% were excluded because of the potential clinopyroxene and magnetite fractionation. Komatiites with MgO > 18 wt.% are also filtered out. (3) Highly altered samples with a loss on ignition higher than 6 wt% or exhibiting significant Ce anomalies (Ce/Ce^* <0.9 or > 1.1)[18] were excluded. (4) Subduction-related and crustally contaminated rocks are generally characterized by negative Nb anomaly, therefore, we selected the samples with $(Nb/La)_{PM} \geq 0.75$ to represent ambient mantle-derived melts[18,48]. (5) Available thermobarometers and V/Ti oxybarometer are designed for peridotite-derived melts[24,27,30], therefore, we only considered lavas with geochemical criteria such as $CaO > 13.81 - 0.274\ MgO$[49] to consider formation from peridotite sources. To obtain meaningful magma compositions, we used the PRIMELT3 software to exclude melts that have undergone fractionation of clinopyroxene and melts derived from CO_2-rich peridotite or pyroxenite sources[49]. Using these filtering criteria, we obtained 76 samples that could represent the primitive melts of ambient mantle ranging in age from 3.8 Ga to 0 Ga. In addition, we also used a database of mantle and orogenic eclogite suites which were carefully filtered by the above criteria[17]. Those samples, along with plume-derived melts were used to decipher the redox and thermal state evolution of the mantle.

Determining the fo_2 of mantle-derived magmas

The fo_2 of ambient mantle-derived melts is estimated by the V/Ti redox proxy, which is advantageous as it is more sensitive to mantle redox conditions and is not affected by residual garnet or volatiles degassing[30]. Because the partition coefficients of both V and Ti in silicate minerals are temperature-dependent, we calculated the melting temperature and pressure of non-arc basalts using a published thermobarometer[27] before fo_2 determination. We assumed that the composition of the mantle peridotite represented a depleted mantle source[50], and the initial mineral assemblage and melting reactions were adopted from ref. 51. The partition coefficients of V, Sc, and Ti for olivine, orthopyroxene, clinopyroxene, and spinel were sourced from ref. 30. Considering the susceptibility of Na content to alteration effects, we utilized the Ti content as a proxy to constrain the degree of partial melting. The detailed fo_2 calculation followed the approach reported in ref. 18. During the calculation process, a partial melting model for spinel peridotite (model A) was employed to determine the oxygen fugacity of samples with melting pressures within the stability range of spinel peridotite. For samples with melting pressures exceeding 2.7 GPa[52], the melting model of garnet peridotite (model B) was employed.

The fo_2 of the plume-derived ultramafic lavas was determined by three updated olivine oxybarometers which calibrate the effects of temperature and melt composition on $D^{Ol/melt}_V$[29,30]. During the calculation, crystallization temperatures of olivine were estimated by the Sc/Y exchange coefficient between olivine and the melt[29].

Recent studies revealed that pervasive degassing and fractional crystallization processes significantly affect the fo_2 of magmas[39,53,54]. Our calculations also show that fo_2 was not constant during the evolutionary process of most mantle-derived magmas. Hence, we selected the most primitive olivine with the highest Fo value as an indicator of the fo_2 of the primary magma (Supplementary Fig. 1). The resulting fo_2 during olivine crystallization calculated by different oxybarometers was in good agreement within the method uncertainties (Supplementary Fig. 2).

Primary melt reconstruction and melting conditions

Reconstructing the composition of the primary melt is a prerequisite for estimating melting conditions[24,27]. The canonical reconstruction method involves adding or subtracting olivine from the whole rock composition until the melt reaches equilibrium with mantle olivine, which is highly effective for systems closed to oxygen such as MORBs[24]. This method was applied to the ambient mantle-derived basalts to determine the melting temperature and pressure of the ambient mantle. During the calculation, we reconstructed the primary melt composition of the MORB-like basalts by adding equilibrium olivine until the melt is in equilibrium with residual olivine (Fo=90[27]). The $Fe^{3+}/\Sigma Fe$ ratios of MORB-like basalts are assumed to be 0.1 and there are only very subtle differences when calculating $Fe^{3+}/\Sigma Fe$ by $Fe_2O_3/TiO_2 = 0.5$[49], which do not affect the conclusions made in this study.

recent studies have revealed that plume-derived magmas are volatile-enriched and that their fo_2 has been significantly modified by degassing[39,55]. Melt inclusions in komatiites reveal that primary komatiites are somewhat enriched in H_2O, and the majority of the H_2O was degassed for Fo <90[26]. Our oxybarometer results also suggest that some Phanerozoic plume-derived magmas were not closed for oxygen (Supplementary Fig. 1). Therefore, an alternative

method for modelling the primary magmas of mantle plume-derived melts is necessary. In this study, we computed the primary melt composition of plume-derived melts by adding olivine stepwise and recalculating the $Fe^{3+}/\Sigma Fe$ ratios of melt according to the oxybarometer result during every step. Specific steps are as follows:

(1) Tentatively predict fo_2 and olivine-melt equilibration temperatures: Supposing that olivines are in equilibrium with a candidate melt composition (whole-rock or melt inclusions) and calculate fo_2 and temperature, using $D^{ol/melt}{}_V$ for fo_2 and $D^{ol/melt}{}_{Sc/Y}$ thermometer for temperature[29].

(2) Equilibrium test: Calculate $Fe^{3+}/\Sigma Fe$ ratio in melt using the parameterization of ref. 56 and predict $K_D(Fe\text{-}Mg)^{Ol\text{-}melt}$ by Equation 8b from ref. 12. Once the $Fe^{3+}/\Sigma Fe$ ratio is determined, the $K_D(Fe\text{-}Mg)^{Ol\text{-}melt}$ can be obtained. The equilibrated melt could yield $K_D(Fe\text{-}Mg)^{Ol\text{-}melt}$ consistent with the predicted value (within 1σ range, ±0.03). The preferred values of fo_2 and temperature are obtained from this equilibrated melt.

(3) Equilibrated melt composition calculation: If the observed $K_D(Fe\text{-}Mg)^{Ol\text{-}melt}$ does not match the predicted value, the melt is disequilibrated with olivine and the candidate melt composition fails. Next, we calculated the melt in equilibrium with the observed olivine. For natural melts along olivine control lines, the equilibrated melt can be calculated by incrementally adding or subtracting olivine and repeating step1–3, until the melt achieves equilibrium with the olivine. The estimated fo_2 is reliable only when the melt is in equilibrium with the observed olivine. It should be noted that the V and Sc concentrations in the melt can be calculated by mass-balance or alternatively by regression[19,26,37].

(4) This iterative calculation ends when the magma is in equilibrium with the most primitive olivine.

After the reconstruction of the primary melt, the melting temperature, melting pressure, and the T_P were estimated by different thermobarometers[24,27,28]. The H_2O contents of the ambient mantle- and plume-derived melts are set to 0.2 wt.% and 0.6 wt.%, respectively[26,57]. All the methods yielded identical results and the estimated T_P was highly correlated with the olivine crystallization temperatures (Supplementary Fig. 3), which proves the rationality of our calculation.

Determining the fo_2 of the mantle source

Similar to the solid mantle, the fo_2 of mantle-derived melts exhibits continuous variations during decompression[42]. Consequently, to accurately determine the fo_2 of the mantle source region, it is imperative to correct the fo_2 of the primary magma to match the thermodynamic conditions of the mantle source region. Here, we initiated the process by calculating the $Fe^{3+}/\Sigma Fe$ in the primary melt using its established correlation with fo_2[56]. Subsequently, assuming that the composition of the melt has not changed since its separation from the peridotite residue, we determined the fo_2 of mantle-derived melts at the thermodynamic conditions prevailing in the source region based on thermobarometer results[27]. The comparison of the results from different methods is shown in Supplementary Fig. 4.

Calculation of potential fo_2

In the adiabatic ascent of mantle peridotite with a given composition, its fo_2 gradually increased with decreasing pressure[20]. During this process, the rate of fo_2 increase is primarily controlled by T_P. Therefore, to calculate the mantle potential fo_2, it is essential to determine the fo_2 characteristics of the mantle peridotite under different temperatures and pressures.

In this study, the oxygen fugacity of the mantle under different temperature and pressure conditions was calculated through the following equilibria:

$$\begin{aligned} &2Ca_3Fe_2Si_3O_{12} + 2Mg_3Al_2Si_3O_{12} + 4FeSiO_3 \\ &= 2Ca_3Al_2Si_3O_{12} + 4Fe_2SiO_4 + 6MgSiO_3 + O_2 \end{aligned} \quad (1)$$

$$\begin{aligned} \log(fo_2) = &-\frac{\Delta G^\circ}{\ln(10)RT} + 2\log(\alpha^{Gt}_{Ca_3Fe_2Si_3O_{12}}) + 2\log(\alpha^{Gt}_{Mg_3Al_2Si_3O_{12}}) \\ &+ 4\log(\alpha^{Opx}_{FeSiO_3}) - 2\log(\alpha^{Gt}_{Ca_3Al_2Si_3O_{12}}) \\ &- 4\log(\alpha^{Ol}_{Fe_2SiO_4}) - 6\log(\alpha^{Opx}_{MgSiO_3}) \end{aligned} \quad (2)$$

Where R is the gas constant, T is the temperature in K, ΔG° is the standard-state change in free energy of the reaction. ΔG° and component activities in Eq. 1 were derived from a previous study[20].

The determination of mantle fo_2 along various adiabats is achieved through the application of Eq. (2). The mineral modes of the garnet peridotite at different pressures are sourced from ref. 58. The compositions of minerals are established by conducting a mass balance, taking into account the aluminum contents of orthopyroxene and clinopyroxene, which are determined from a combination of experimental and natural data[59,60]. Additionally, the experimental Fe-Mg partitioning data[60,61] was utilized to determine the mineral compositions. The distribution of Fe^{3+} among garnet, orthopyroxene, and clinopyroxene was ascertained through Fe^{3+} partitioning models derived from analyses of natural xenoliths[59].

Thermodynamic calculations revealed that the rate of fo_2 increase during adiabatic ascent ($K(fo_2)$) varied with T_P. For instance, as pressure decreases along an adiabat of 1300 °C, the fo_2 for a given bulk rock composition will increase with a rate of 0.51 log unit/GPa. In contrast, at a T_P of 1800 °C, the $K(fo_2)$ value is 0.35 log unit/GPa (Supplementary Fig. 5). For computational convenience, we established a functional relationship between $K(fo_2)$ and mantle potential temperature:

$$K(fo_2) = 2.48\times10^{-7}(T_P)^2 - 1.09\times10^{-3}T_P + 1.51 \quad (3)$$

Where, T_P is in °C.

Eventually, the formula for calculating mantle potential oxygen fugacity is:

$$fo_{2P} = fo_2(source) + K(fo_2)(P-1) \quad (4)$$

Where fo_2 (source) is the oxygen fugacity of the mantle source with respect to the FMQ buffer and P is the melting pressure in GPa.

The uncertainty in calculating mantle potential fo_2 primarily arises from errors in magmatic fo_2 calculations (~0.3 log units) and uncertainties in calculating melting pressure (20%). To determine the total error associated with calculating the mantle potential fo_2, we employed a Monte Carlo simulation ($N = 10000$) to constrain the uncertainties at each step of the calculation and assessed their cumulative impact on the final results. The procedural steps include:

(1) fo_2 calculation errors of $D^{Ol/melt}{}_V$ oxybarometers and V/Ti redox proxy: 0.37 and 0.51 log units, respectively.

(2) T_P error of 42 °C and partial melting pressure error of 20%[27].

(3) Errors in correcting melt fo_2 at 1 atm to the source region conditions: 0.12 log unit[62].

(4) The uncertainty associated with $K(fo_2)$ estimation is 0.04 log unit/GPa.

Monte Carlo simulation results indicate that, owing to the significant error in the melting pressure of Archean komatiite rocks (~1 GPa), the final error in calculating the mantle potential fo_2 propagates to ~0.7 log units. In contrast, despite a larger error in the V/Ti

redox proxy (~0.5 log units), the final error in mantle potential oxygen fugacity was slightly less at ~0.6 log units. This discrepancy is attributed to the fact that melts derived from the ambient mantle exhibit shallow melting pressures.

Estimating the fo_2 of Hadean crust

To estimate the fo_2 of the Hadean crust, we established a functional relationship between the fo_2 of the mantle-derived magmas and T_P (Fig. 2).

$$\text{Plume}: fo_2\,(\Delta\text{FMQ}) = 7.48\,(\pm 0.70) - 0.00491\,(\pm 0.00046) \times T_P \quad (5)$$

$$\text{Ambient mantle}: fo_2\,(\Delta\text{FMQ}) = 6.68(\pm 0.97) - 0.0052(\pm 0.00065) \times T_P \quad (6)$$

Here, fo_2 is the fo_2 of mantle-derived melts expressed in ΔFMQ, T_P is the mantle potential temperature in °C. The possible mantle potential temperature in the Hadean was inferred from the low-Urey-ratio model with Urey ratios of 0.08 to 0.34[11,33].

Data availability

The calculated oxygen fugacity data generated in this study are available as Supplementary Data 1 and have been deposited in the Figshare repository (https://doi.org/10.6084/m9.figshare.25181621).

References

1. Kasting, J. F. Earth's early atmosphere. *Science* **259**, 920–926 (1993).
2. Hirschmann, M. M. Magma ocean influence on early atmosphere mass and composition. *Earth Planet. Sci. Lett.* **341-344**, 48–57 (2012).
3. Holland, H. D. Volcanic gases, black smokers, and the great oxidation event. *Geochim. Cosmochim. Acta* **66**, 3811–3826 (2002).
4. Moussallam, Y., Oppenheimer, C. & Scaillet, B. On the relationship between oxidation state and temperature of volcanic gas emissions. *Earth Planet. Sci. Lett.* **520**, 260–267 (2019).
5. Walter, M. J. Melting of garnet peridotite and the origin of komatiite and depleted lithosphere. *J. Petrol.* **39**, 29–60 (1998).
6. Dasgupta, R. et al. Carbon-dioxide-rich silicate melt in the Earth's upper mantle. *Nature* **493**, 211–215 (2013).
7. Frost, D. J. & McCammon, C. A. The redox state of Earth's mantle. *Annu. Rev. Earth Planet. Sci.* **36**, 389–420 (2008).
8. Kadoya, S., Catling, D. C., Nicklas, R. W., Puchtel, I. S. & Anbar, A. D. Mantle data imply a decline of oxidizable volcanic gases could have triggered the Great Oxidation. *Nat. Commun.* **11**, 2774 (2020).
9. Korenaga, J. Urey ratio and the structure and evolution of Earth's mantle. *Rev. Geophys.* **46**, RG2007 (2008).
10. Davies, G. F. Effect of plate bending on the Urey ratio and the thermal evolution of the mantle. *Earth Planet. Sci. Lett.* **287**, 513–518 (2009).
11. Herzberg, C., Condie, K. & Korenaga, J. Thermal history of the Earth and its petrological expression. *Earth Planet. Sci. Lett.* **292**, 79–88 (2010).
12. Putirka, K. Rates and styles of planetary cooling on Earth, Moon, Mars, and Vesta, using new models for oxygen fugacity, ferric-ferrous ratios, olivine-liquid Fe-Mg exchange, and mantle potential temperature. *Am. Mineral.* **101**, 819–840 (2016).
13. Canil, D. Vanadium partitioning and the oxidation state of Archaean komatiite magmas. *Nature* **389**, 842–845 (1997).
14. Kuwahara, H. & Nakada, R. Partitioning of Fe^{2+} and Fe^{3+} between bridgmanite and silicate melt: Implications for redox evolution of the Earth's mantle. *Earth Planet. Sci. Lett.* **615**, 118197 (2023).
15. Anser Li, Z.-X. & Aeolus Lee, C.-T. The constancy of upper mantle fO_2 through time inferred from V/Sc ratios in basalts. *Earth Planet. Sci. Lett.* **228**, 483–493 (2004).
16. Trail, D., Watson, E. B. & Tailby, N. D. The oxidation state of Hadean magmas and implications for early Earth's atmosphere. *Nature* **480**, 79–82 (2011).
17. Aulbach, S. & Stagno, V. Evidence for a reducing Archean ambient mantle and its effects on the carbon cycle. *Geology* **44**, 751–754 (2016).
18. Gao, L. et al. Oxidation of Archean upper mantle caused by crustal recycling. *Nat. Commun.* **13**, 3283 (2022).
19. Nicklas, R. W. et al. Secular mantle oxidation across the Archean-Proterozoic boundary: Evidence from V partitioning in komatiites and picrites. *Geochim. Cosmochim. Acta* **250**, 49–75 (2019).
20. Stagno, V., Ojwang, D. O., McCammon, C. A. & Frost, D. J. The oxidation state of the mantle and the extraction of carbon from Earth's interior. *Nature* **493**, 84–88 (2013).
21. Gaillard, F., Scaillet, B., Pichavant, M. & Iacono-Marziano, G. The redox geodynamics linking basalts and their mantle sources through space and time. *Chem. Geol.* **418**, 217–233 (2015).
22. Rohrbach, A. & Schmidt, M. W. Redox freezing and melting in the Earth's deep mantle resulting from carbon-iron redox coupling. *Nature* **472**, 209–212 (2011).
23. Miller, W. G. R., Holland, T. J. B. & Gibson, S. A. Garnet and Spinel Oxybarometers: New internally consistent multi-equilibria models with applications to the oxidation state of the lithospheric mantle. *J. Petrol.* **57**, 1199–1222 (2016).
24. Herzberg, C. & Asimow, P. D. PRIMELT3 MEGA.XLSM software for primary magma calculation: Peridotite primary magma MgO contents from the liquidus to the solidus. *Geochem. Geophys. Geosyst.* **16**, 563–578 (2015).
25. Keller, B. & Schoene, B. Plate tectonics and continental basaltic geochemistry throughout Earth history. *Earth Planet. Sci. Lett.* **481**, 290–304 (2018).
26. Sobolev, A. V. et al. Komatiites reveal a hydrous Archaean deep-mantle reservoir. *Nature* **531**, 628–632 (2016).
27. Lee, C.-T. A., Luffi, P., Plank, T., Dalton, H. & Leeman, W. P. Constraints on the depths and temperatures of basaltic magma generation on Earth and other terrestrial planets using new thermobarometers for mafic magmas. *Earth Planet. Sci. Lett.* **279**, 20–33 (2009).
28. Sun, C. & Dasgupta, R. Thermobarometry of CO_2-rich, silica-undersaturated melts constrains cratonic lithosphere thinning through time in areas of kimberlitic magmatism. *Earth Planet. Sci. Lett.* **550**, 116549 (2020).
29. Mallmann, G. & O'Neill, H. S. C. Calibration of an empirical thermometer and oxybarometer based on the partitioning of Sc, Y and V between Olivine and silicate melt. *J. Petrol.* **54**, 933–949 (2013).
30. Wang, J. et al. Oxidation state of arc mantle revealed by partitioning of V, Sc, and Ti between mantle minerals and basaltic Melts. *J. Geophys. Res.: Solid Earth* **124**, 4617–4638 (2019).
31. Zhang, F. et al. The Redox state of the asthenospheric mantle and the onset of melting beneath mid-ocean ridges. *J. Geophys. Res.: Solid Earth* **129**, e2023JB027033 (2024).
32. Herzberg, C. & Gazel, E. Petrological evidence for secular cooling in mantle plumes. *Nature* **458**, 619–622 (2009).
33. Korenaga, J. Initiation and evolution of plate tectonics on Earth: Theories and observations. *Annu. Rev. Earth Planet. Sci.* **41**, 117–151 (2013).
34. Sun, W.-D. et al. Carbonated mantle domains at the base of the Earth's transition zone. *Chem. Geol.* **478**, 69–75 (2018).
35. Herzberg, C. & O'Hara, M. J. Plume-associated ultramafic magmas of Phanerozoic Age. *J. Petrol.* **43**, 1857–1883 (2002).
36. Berry, A. J. et al. Oxidation state of iron in komatiitic melt inclusions indicates hot Archaean mantle. *Nature* **455**, 960–963 (2008).

37. Nicklas, R. W., Puchtel, I. S. & Ash, R. D. Redox state of the Archean mantle: Evidence from V partitioning in 3.5–2.4 Ga komatiites. *Geochim. Cosmochim. Acta* **222**, 447–466 (2018).
38. Wu, Y. D. et al. Redox heterogeneity of picritic lavas with respect to their mantle sources in the Emeishan large igneous province. *Geochim. Cosmochim. Acta* **320**, 161–178 (2022).
39. Moussallam, Y. et al. Mantle plumes are oxidised. *Earth Planet. Sci. Lett.* **527**, 115798 (2019).
40. McKenzie, D. & Bickle, M. J. The volume and composition of melt generated by extension of the lithosphere. *J. Petrol.* **29**, 625–679 (1988).
41. Wade, J. & Wood, B. J. Core formation and the oxidation state of the Earth. *Earth Planet. Sci. Lett.* **236**, 78–95 (2005).
42. Armstrong, K., Frost, D. J., McCammon, C. A., Rubie, D. C. & Ballaran, T. B. Deep magma ocean formation set the oxidation state of Earth's mantle. *Science* **365**, 903–906 (2019).
43. Deng, J., Du, Z., Karki, B. B., Ghosh, D. B. & Lee, K. K. M. A magma ocean origin to divergent redox evolutions of rocky planetary bodies and early atmospheres. *Nat. Commun.* **11**, 2007 (2020).
44. Kuwahara, H., Nakada, R., Kadoya, S., Yoshino, T. & Irifune, T. Hadean mantle oxidation inferred from melting of peridotite under lower-mantle conditions. *Nat. Geosci.* **16**, 461–465 (2023).
45. Marras, G., Mikhailenko, D., McCammon, C. A., Agasheva, E. & Stagno, V. Ferric Iron in Eclogitic Garnet and Clinopyroxene from the V. Grib Kimberlite Pipe (NW Russia): Evidence of a Highly Oxidized Subducted Slab. *J. Petrol.* **65**, egae054 (2024).
46. Wang, R., Wu, S. C., Weinberg, R. F., Collins, W. J. & Cawood, P. A. Zircons reveal the history of fluctuations in the oxidation state of crustal magmatism and supercontinent cycle. *Sci. Bull.* **69**, 97–102 (2024).
47. Sobolev, A. V. et al. Deep hydrous mantle reservoir provides evidence for crustal recycling before 3.3 billion years ago. *Nature* **571**, 555–559 (2019).
48. Liu, H., Zartman, R. E., Ireland, T. R. & Sun, W. D. Global atmospheric oxygen variations recorded by Th/U systematics of igneous rocks. *Proc. Natl Acad. Sci. USA* **116**, 18854–18859 (2019).
49. Herzberg, C. & Asimow, P. D. Petrology of some oceanic island basalts: PRIMELT2.XLS software for primary magma calculation. *Geochem. Geophys. Geosyst.* **9**, Q09001 (2008).
50. Salters, V. J. M. & Stracke, A. Composition of the depleted mantle. *Geochem. Geophys. Geosyst.* **5**, Q05B07 (2004).
51. Workman, R. K. & Hart, S. R. Major and trace element composition of the depleted MORB mantle (DMM). *Earth Planet. Sci. Lett.* **231**, 53–72 (2005).
52. Robinson, J. A. C. & Wood, B. J. The depth of the spinel to garnet transition at the peridotite solidus. *Earth Planet. Sci. Lett.* **164**, 277–284 (1998).
53. Burgisser, A. & Scaillet, B. Redox evolution of a degassing magma rising to the surface. *Nature* **445**, 194–197 (2007).
54. Cottrell, E. & Kelley, K. A. The oxidation state of Fe in MORB glasses and the oxygen fugacity of the upper mantle. *Earth Planet. Sci. Lett.* **305**, 270–282 (2011).
55. Brounce, M., Stolper, E. & Eiler, J. Redox variations in Mauna Kea lavas, the oxygen fugacity of the Hawaiian plume, and the role of volcanic gases in Earth's oxygenation. *Proc. Natl Acad. Sci. USA* **114**, 8997–9002 (2017).
56. Kress, V. C. & Carmichael, I. S. E. The compressibility of silicate liquids containing Fe_2O_3 and the effect of composition, temperature, oxygen fugacity and pressure on their redox states. *Contribut. Mineral. Petrol.* **108**, 82–92 (1991).
57. Saal, A. E., Hauri, E. H., Langmuir, C. H. & Perfit, M. R. Vapour undersaturation in primitive mid-ocean-ridge basalt and the volatile content of Earth's upper mantle. *Nature* **419**, 451–455 (2002).
58. Hirschmann, M. M., Tenner, T., Aubaud, C. & Withers, A. C. Dehydration melting of nominally anhydrous mantle: The primacy of partitioning. *Phys. Earth Planet. Inter.* **176**, 54–68 (2009).
59. Canil, D. & O'Neill, H. S. C. Distribution of ferric iron in some upper-mantle assemblages. *J. Petrol.* **37**, 609–635 (1996).
60. Balta, J. B., Asimow, P. D. & Mosenfelder, J. L. Hydrous, low-carbon melting of Garnet Peridotite. *J. Petrol.* **52**, 2079–2105 (2011).
61. O'Neill, H. S. C. & Wood, B. J. An experimental study of Fe-Mg partitioning between garnet and olivine and its calibration as a geothermometer. *Contribut. Mineral. Petrol.* **70**, 59–70 (1979).
62. Birner, S. K., Cottrell, E., Warren, J. M., Kelley, K. A. & Davis, F. A. Peridotites and basalts reveal broad congruence between two independent records of mantle fO2 despite local redox heterogeneity. *Earth Planet. Sci. Lett.* **494**, 172–189 (2018).
63. Zhang, H. L., Cottrell, E., Solheid, P. A., Kelley, K. A. & Hirschmann, M. M. Determination of $Fe^{3+}/\Sigma Fe$ of XANES basaltic glass standards by Mössbauer spectroscopy and its application to the oxidation state of iron in MORB. *Chem. Geol.* **479**, 166–175 (2018).
64. Nicklas, R. W., Puchtel, I. S. & Baxter, E. F. Concordance of V-in-olivine and Fe-XANES oxybarometry methods in mid-ocean ridge basalts. *Earth Planet. Sci. Lett.* **625**, 118492 (2024).
65. Smithies, R. H. et al. Oxygen isotopes trace the origins of Earth's earliest continental crust. *Nature* **592**, 70–75 (2021).

Acknowledgements

We acknowledge Sonja Aulbach for providing the eclogite data. We thank Lihui Chen and Vadim Kamenetsky for their valuable discussions. We are also grateful to Robert Nicklas for thoughtful and critical comments, which significantly improved this paper. F.Z. is funded by NSFC (42303054), H.L. is funded by NSFC (42373003), W.S. is funded by NSFC (92258303), the Laoshan Laboratory (LSKJ202204100), and the Taishan Scholar Program of Shandong (tspd20230609). V.S. is funded by HERMES project n. 2022R35X8Z.

Author contributions

F.Z. conceptualized the idea, compiled and modeled the geochemical data, and drafted the initial version of the manuscript. W.S. and V.S. contributed to data collection and the development of ideas. All authors including L.Z., C.C., H.L. and C.L. were involved in the revision of the manuscript.

Competing interests

The authors declare no competing interests.

Additional information

Supplementary information The online version contains supplementary material available at https://doi.org/10.1038/s41467-024-50778-z.

Correspondence and requests for materials should be addressed to Fangyi Zhang or Weidong Sun.

Peer review information *Nature Communications* thanks Robert Nicklas, and the other, anonymous, reviewer(s) for their contribution to the peer review of this work. A peer review file is available.